

1 **Climatic characteristics of the Jianghuai cyclone and its linkage with**
2 **precipitation during the Meiyu period from 1961 to 2020**

3 Ran Zhu¹, Lei Chen^{1,2}

4 ¹Department of Atmospheric Science, School of Environmental Studies, China University of
5 Geosciences, Wuhan, 430074, China

6 ²Centre for Severe Weather and Climate and Hydro-Geological Hazards, Wuhan, 430074, China

7 Correspondence to: Lei Chen (leichen@cug.edu.cn)

8 **Abstract.** This study examines the climatic characteristics of 202 Jianghuai cyclones
9 and their linkage with precipitation during the Meiyu period from 1961 to 2020. The
10 results show that cyclones mainly originate from eastern Hubei Province and south-
11 central Anhui Province, and further explored the statistical characteristics of the
12 strength, radius, and their positive correlation. When studying the interdecadal variation
13 of cyclones, we found that there is a similar trend between the interdecadal variation of
14 cyclones and Meiyu precipitation. Therefore, we further investigate the correlation
15 between the Jianghuai cyclones and the precipitation during the Meiyu period. There is
16 a positive correlation coefficient of 0.769 between them. It's worth mentioning that the
17 percentage of precipitation affected by cyclone activities can reach up to 47%. The
18 anomalous increase in precipitation caused by cyclones above 27°N can reach a
19 maximum of 7 mm/day. When the cyclone existed, there was a significant altitude
20 anomaly of negative geopotential height can be traced to day -4 at the 500 hPa level
21 over Mongolia. The abnormally enhanced WPSH, southwest jet and negative
22 geopotential height are the dominant factors causing abnormal precipitation during
23 Jianghuai cyclones. Before and after the cyclone developed, water vapor flux and
24 divergence from low latitudes abnormally increased. These provide sufficient water
25 vapor conditions for the generation of cyclone precipitation.

1. Introduction

Meiyu is a special rainy season due to the progress of the East Asian summer monsoon. The East Asian summer monsoon broke out in the South China Sea in mid-May and then advanced northward, forming rain bands in South China, the Jianghuai region, the Korean Peninsula and Japan (Ding et al., 2004,2007; Qian et al., 2000). The name for this special rainy season is called Meiyu in China, while it is called Changma in South Korea and it is called Baiu in Japan (Ninomiya et al., 1987; Oh et al., 1997; Saito. 1995;). Meiyu front is one of the important weather systems affecting summer precipitation in the middle and lower reaches of the Yangtze River (Pang et al., 2013; Wang et al., 2014; Zhou et al., 2022; Tao et al., 1979). From mid-June to early July, the east of Yichang, Hubei Province, has continuous rains and short sunshine. These conditions are accompanied by heavy rainfall, strong wind and other weather phenomena in these areas during the Meiyu period (Ding. 1992; Zhao et al., 2021; Zhou et al., 2017). In China, the mean annual precipitation during the Meiyu period in the Jianghuai River Basin can reach 300 mm, accounting for 30%-40% of the mean annual total precipitation, and even up to 500 mm or more in the extreme Meiyu period (Liu et al., 2020). Historically, most of the summer floods disasters are caused by precipitation anomalies in the Meiyu period. Some scholars have studied and analyzed the representative floods of 1996, 1998, 2016 and 2020 (Bao et al., 2021; Su et al., 2021; Zhao et al., 2018; Zhong et al., 2023). These floods, caused by the Meiyu front, had adverse effects on people's safety, lives and property (Yan et al., 2021). Scholars in China have divided rainstorms caused by Meiyu fronts into three types (Zhang et al., 2004). The first type is the β mesoscale convective rainstorm on the Meiyu front. This type of rainstorm has a range of less than 300 km with strong intensity and a fast formation process (He et al., 2007). It is difficult to forecast before 12 hours and can be detected only by using radar to make a proximity forecast (Zhang et al., 2002). The second type is the persistent rainstorm located in front of the high-altitude low-pressure tank in the western part of the Meiyu front. It is characterized by a long duration of approximately 5 days but appears less frequently, mainly in western Hubei and western

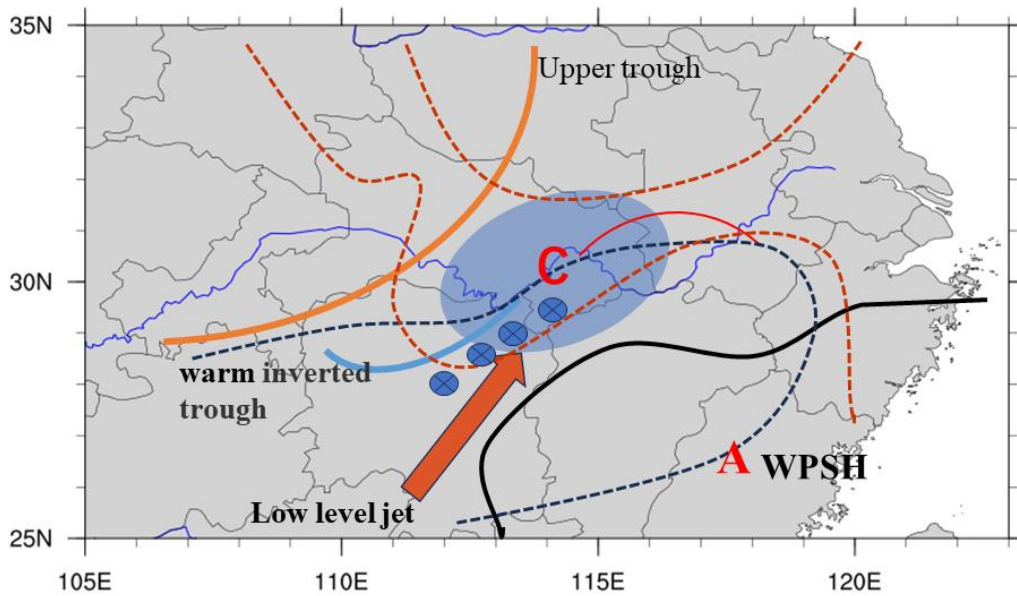
55 Hunan and Sichuan (Cai et al., 2021; Wu et al., 2020;). The last type is the rainstorm
56 caused by the Jianghuai cyclone located east of the origin of the Meiyu. The Jianghuai
57 cyclones are affected by the thermal conditions of the sea and land and likely occur in
58 the eastern part of the Meiyu front (Wang et al., 2016). The positive vorticity advection
59 in front of the high-altitude trough and the warm advection in front of the front promote
60 the eastward movement and development of the cyclone (Shen et al., 2019; Zhang et
61 al., 2016). During the development of the cyclone, the lower levels are dominated by
62 the southwest warm and humid airflow, and the high levels are mainly affected by dry
63 and cold air (Zhao et al., 2008). This type of rainstorm has a large range, high intensity
64 and long duration of precipitation (Wang et al., 2012; Xu et al., 2011).

65 Scholars' studies on Jianghuai cyclones during the Meiyu period were initially
66 based on individual case analysis. Xu et al. (2013) studied a cyclone process in 2011
67 and found that the cyclone process lasted up to 36 h. The cyclone rainstorm was
68 distributed on the south side of the cyclone. Heavy precipitation during the whole
69 cyclone mainly occurred in the lower reaches of the Yangtze River. Wu et al. (2020)
70 studied 2 different cyclone rainstorm processes. They found that rainfall is directly
71 proportional to cyclone intensity. There is a strong convergence center of water vapor
72 flux during cyclone development. Zhou et al. (2020) found that a tornado was generated
73 from the cyclone occlusion stage on July 22. The tornado was under the influence of a
74 strong and fast Jianghuai cyclone and produced heavy precipitation accompanied by
75 thunderstorm phenomena. With the improvement of cyclone identification methods and
76 reconstruction of reanalysis data, statistical studies of cyclones have been further
77 developed (Simmonds et al., 1999; 2000; Wernli et al., 2006). Yang et al. (2010)
78 modeled the rainstorm process in the lower reaches of the Yangtze River from 1998 to
79 2005. The cyclones accounted for 62.5% of the rainstorm cases, and more than 70% of
80 the cyclones could develop and produce rainstorms. The Jianghuai cyclone located in
81 the lower reaches of the Yangtze River generally exists in the lower troposphere at 700
82 hPa. The horizontal scale is within 400 km, and the life period on land is generally less
83 than 48 h. Wang et al. (2015) found that the number of cyclones was lower and their

84 intensity was weak in the 1980s and 1990s. In the early 2000s, cyclones were more
85 frequent, and their intensity increased. After 2010, there was again a decreasing trend.
86 Zhang et al. (2018) divided 60 cases of extreme precipitation in the middle reaches of
87 the Yangtze River from 2008 to 2015 into five types. Among them, the extreme
88 precipitation of the Jianghuai cyclone type accounted for 30%. The stable and
89 maintained Western Pacific subtropical high (WPSH) system is one of the important
90 reasons for the strong precipitation produced by cyclones. Because of the weak cold air
91 force, the intensity of the Jianghuai cyclone is weaker than that in spring (Zhou et al.,
92 2017). The daily analysis of the Jianghuai cyclones in the Meiyu period is easy to ignore.
93 All these studies indicate that the Jianghuai cyclone is an important weather system that
94 causes heavy rainfall during the Meiyu period in the middle and lower reaches of the
95 Yangtze River (Wu et al., 2021; Zhang et al., 2018; Zhu et al., 1998).

96 Research on the climatic characteristics and precipitation effects of Jianghuai
97 cyclones during the Meiyu period in the past 60 years has not yielded clear results. In
98 this study, the relative vorticity method is used to objectively identify and track
99 cyclones based on reanalysis data provided by ERA5. The climatological characteristics
100 of the Jianghuai cyclones during this period are studied. We analyze the correlation
101 between Jianghuai cyclone activity and precipitation. This study provides a reference
102 for the long-term and short-term forecasting of precipitation in the Meiyu period.

103 The remainder of the present paper is organized as follows. Section 2 of this paper
104 presents the dataset and analytical methods. In Section 3, we show the climatology
105 composite of the cyclone tracks, genesis locations, intensity, lifetime and so on. There
106 is a positive correlation between the frequency of cyclonic activity and precipitation in
107 the Meiyu period. The relationship between them is studied by means of the
108 geopotential height anomaly and water vapor flux anomaly. Section 4 provides the main
109 discussion and findings of this study.



110

111 Fig.1 Schematic diagram of the main weather system and the structure of temperature
 112 and pressure field in the middle and low levels of the Jianghuai cyclone. (Red dotted
 113 line: isotherm; Solid black line: contour line; Blue dot: precipitation area; Solid orange
 114 line: 500 hPa upper-level trough; Red arrow: low level jet; Black dotted line: warm
 115 inverted trough; Solid red line: warm shear; Solid blue line: cold shear; Letter C:
 116 cyclone; Letter A: WSPH.)

117 2. Data and methods

118 2.1 Data

119 The time span of all the data is 60 years from 1961 to 2020, and the study area is
 120 located at 108°E-123°E, 27°N-34°N. We use the ERA5 relative vorticity hourly data
 121 (850 hPa) released by the European Centre for Medium Range Weather Forecasts
 122 (ECMWF) for Jianghuai cyclone identification and tracking. The spatial resolution of
 123 the data is 0.25°×0.25°, and the temporal resolution is 6 h. Every 6 h was defined as a
 124 step. The data of geopotential height, wind field, and specific humidity are daily data
 125 processed from ERA5 hourly data with a spatial resolution of 0.25°×0.25° (Hersbach
 126 et al., 2018). The geopotential height and wind field data include pressure levels of
 127 approximately 500 hPa, 700 hPa and 850 hPa. The specific humidity data include

128 pressure levels of approximately 500 hPa, 700 hPa and 850 hPa. The precipitation data
129 are from the CN05.1 grid point observation dataset compiled by the National
130 Meteorological Information Center of China Meteorological Administration with a
131 resolution of $0.25^{\circ} \times 0.25^{\circ}$.

132 We used the Meiyu intensity index to characterize the strength of Meiyu, and data
133 is from the National Climate Center of China. The Meiyu intensity index is defined as:

$$134 \quad M = \frac{L}{L_0} + \frac{0.5(R/L)}{R_0/L_0} + \frac{R}{R_0} - 2.5$$

135 M is the Meiyu intensity index. L is the length of the Meiyu in a given year (unit:
136 day) and L_0 means the average length of the Meiyu over the years (units: day). R is the
137 total precipitation of Jianghuai River basin during Meiyu in a given year, and R_0 is the
138 average total precipitation of Jianghuai River basin during Meiyu over the years. The
139 average period is from 1961 to the current year. For example, L_0 and R_0 values for 2000
140 are the averages from 1961 to 2000. Where M between -0.375 and 0.375, China
141 Meteorological Administration defines this year as the normal. Where M between 0.375
142 and 1.25, this year is defined as a little strong. Where M greater than or equal to 1.25,
143 this year is defined as strong. Where M between -1.25 and -0.375, this year is defined
144 as a little weak. Where M less than or equal to -1.25, this year is defined as weak (GB/T
145 33671-2017).

146 **2.2 Methods**

147 The objective identification and tracking method for cyclones used in this paper is
148 the vorticity tracking method proposed by Hodges (1994, 1995). The first step is to use
149 the relative vorticity field at the 850 hPa pressure level corresponding to every moment
150 of the cyclone to determine the range of each cyclone. The second step is to find the
151 feature points. In the process of finding the feature points, the extreme point and the
152 centroid point are the alternatives. Corresponding to the global relative vorticity grid
153 data of each time point, several feature points can be found, and each point represents
154 a cyclone. The third step is to match the track of each cyclone under the given time
155 span. In Hodges (1994), the assumed data used are defined on a rectangular grid, and

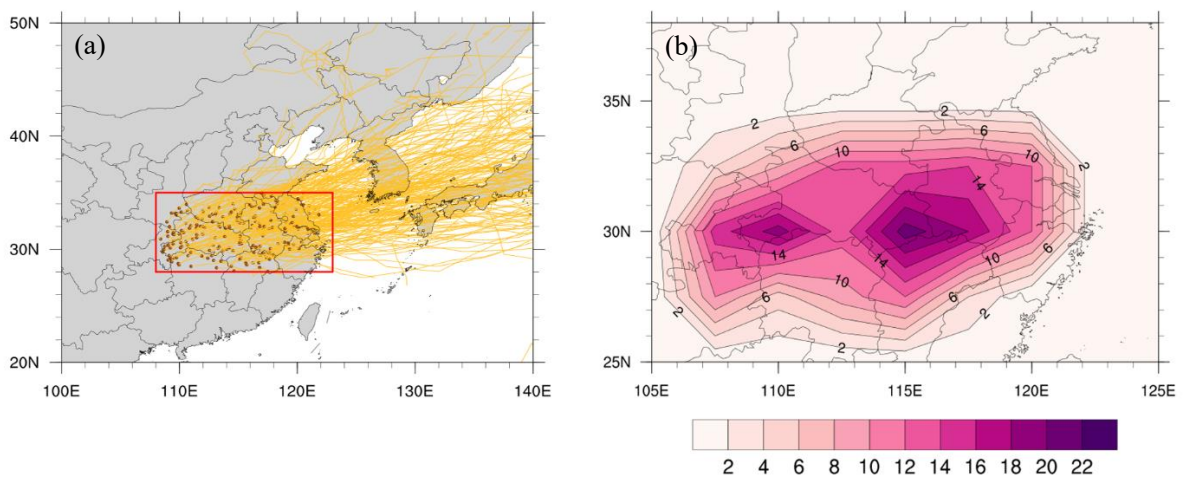
156 each time step is initially processed to identify the maximum or minimum value of the
157 "object" on the positioning grid. The tracking method is feasible on high-resolution
158 grids, but on low-resolution grids, the feature points may not be sufficient to produce
159 smooth trajectories, so the smoothness of the tracking algorithm is effectively limited.
160 Hodges (1995) proposed tracking feature points on the unit sphere, which would
161 become the feature point matching problem of grid data for adjacent time points in
162 cyclone tracking. If the algorithm is reasonable, there is no "discontinuity" mutation in
163 the final arriving cyclone track, and the track is more accurate.

164 In addition to the relative vorticity method of tracking proposed by Hodges,
165 different methods of cyclone identification have also been proposed by other scholars.
166 Lu (2017) improved the extratropical cyclone identification and tracking method
167 involving the nine-point pressure minimum. Jiang et al. (2020) proposed an algorithm
168 for identifying extratropical cyclones on the basis of gridded data. This algorithm is
169 named the eight-section slope detection method. Among them, the most commonly
170 used cyclone tracking methods are the mean sea level pressure method (SLP) and 850
171 hPa relative vorticity method. Mailier et.al (2006) and Zhang et.al (2012) studied the
172 tracks of individual cyclones in these two methods. Both of them found 850 hPa relative
173 vorticity method can identify and detect cyclone center earlier than the SLP method
174 (Mailier et al., 2006). The reason for this result is that SLP is easily affected by
175 topography and large-scale background circulation shear vorticity (Hodges, 1994). So
176 based on this advantage of the relative vorticity method, we select the 850 hPa relative
177 vorticity tracking method. The relative vorticity tracking method can detect low vortex
178 systems earlier and track cyclones for a longer period of time with better stability. When
179 the closed pressure levels are not visible on the satellite map, the vorticity tracking
180 method can still continue to track the cyclone, improving the accuracy of cyclone track
181 data.

182 **3. Results**

183 **3.1 Climatic characteristics of the Jianghuai cyclone during the Meiyu period**

184 A total of 202 Jianghuai cyclones existed during the Meiyu period from 1961 to
 185 2020. The range of cyclone genesis locations defined by the Jiangsu Meteorological
 186 Administration (2017) and the characteristics of the relative vorticity tracking method
 187 were used. We adjust the genesis location and remove the cyclones that are generated
 188 at sea and have no effect on land precipitation (108°E - 123°E , 28°N - 35°N). Figure 2a
 189 shows the distribution of Jianghuai cyclone tracks. The brown dots represent the genesis
 190 locations of the first occurrence of the Jianghuai cyclone. The yellow lines indicate the
 191 tracks of the cyclones. As shown in the figure, the tracks of the cyclone are mainly
 192 eastward and northeast. These two kinds of tracks are related to the upper-level guide
 193 airflow of 500~700 hPa (Wei et al., 2013). The northeast track is mainly due to the
 194 southwest warm and moist air on the edge of the WPSH. The east track is mainly related
 195 to the location of the WPSH. Figure 2b shows the frequency of cyclone occurrence
 196 refers to the total number of cyclones during the Meiyu period from 1961 to 2020. The
 197 genesis locations of cyclones are mainly located in the middle and lower reaches of the
 198 Yangtze River and the Huaihe River basin, with an east–west band distribution (Wang
 199 et al., 2015; Wu et al., 2021). The frequency of occurrence refers to the total number of
 200 cyclones during the Meiyu period from 1961 to 2020 is higher in the region of the Hubei
 201 and Chongqing junction, eastern Hubei, northern Jiangxi, south-central Anhui, Jiangsu
 202 and Zhejiang. Research has found that the genesis locations of cyclones are closely
 203 related to the landform (Xu 2021; Zhang et al., 2012).



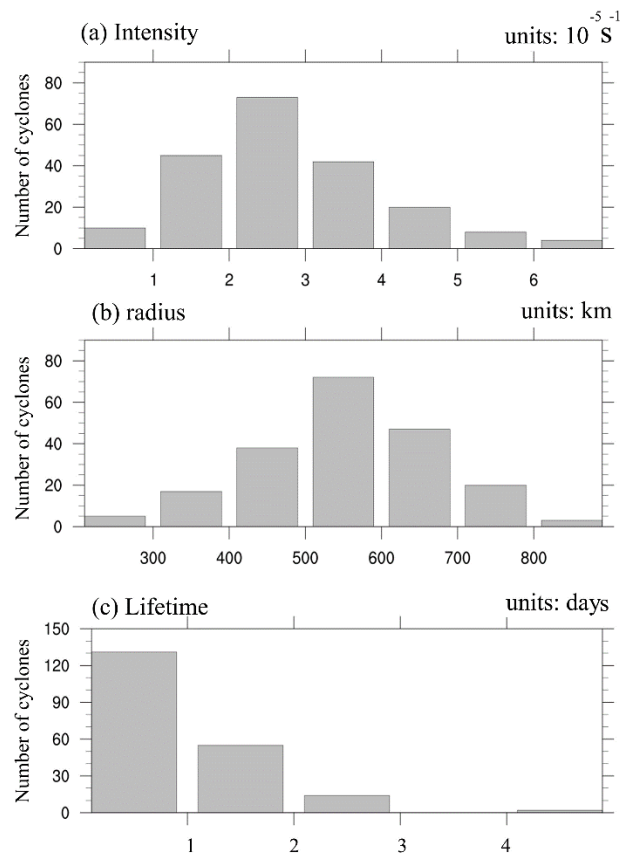
204 Fig 2. Distribution of the cyclone genesis locations, tracks (a) and the frequency of

205 genesis locations refers to the total number of cyclones (b) during the Meiyu period
206 from 1961 to 2020 (The brown dots represent the genesis locations. The yellow lines
207 indicate the tracks).

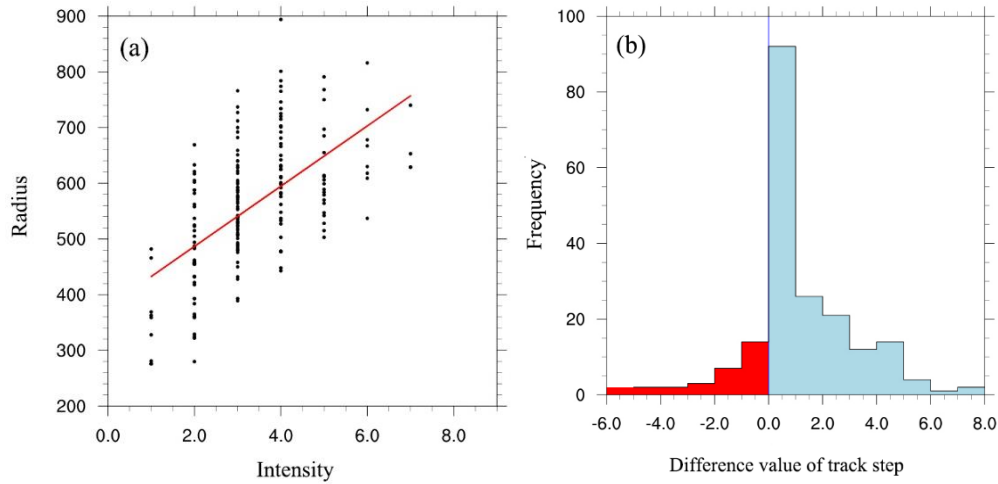
208 To examine the climatological characteristics of Jianghuai cyclones over 60 years,
209 we focus on the intensity, radius, and lifetime of cyclones on land. The intensity of the
210 Jianghuai cyclone is defined as the relative vorticity intensity of the 850 hPa cyclone
211 center. The larger the relative vorticity intensity is, the stronger the cyclone intensity is.
212 Figure 3a shows that among the 202 selected cyclones, the intensity of the cyclone
213 center mainly ranges from $0 \times 10^{-5} \text{ s}^{-1}$ to $7 \times 10^{-5} \text{ s}^{-1}$. When the intensity of the cyclone
214 center is less than $3 \times 10^{-5} \text{ s}^{-1}$, the number of cyclones increases with increasing intensity;
215 when it is larger than $3 \times 10^{-5} \text{ s}^{-1}$, the number of cyclones decreases with weakening
216 intensity. The number of cyclones in the range of $2 \times 10^{-5} \text{ s}^{-1}$ to $3 \times 10^{-5} \text{ s}^{-1}$ has the largest
217 proportion, accounting for 36% of the total number of cyclones. A total of 180 cyclones
218 are in the range of $1 \times 10^{-5} \text{ s}^{-1}$ to $5 \times 10^{-5} \text{ s}^{-1}$ in intensity, accounting for 89%. Figure 3b
219 shows the relationship between the radius of cyclones and the number of cyclones. Most
220 of the cyclones have an average radius between 300 and 800 km, accounting for 96%
221 of the total number. The number of cyclones with radii between 500 and 600 km is the
222 largest, accounting for 35%. Figure 3c shows the relationship between the time of
223 cyclones affecting precipitation on land and the number of cyclones. Most of the
224 cyclones affect precipitation on land for 1-3 days, and only one cyclone affects
225 precipitation on land for more than 3 days. The number of cyclones that affected
226 precipitation on land within 2 days was 186, accounting for 92% of the total number.

227 The intensity of a cyclone is one of the factors affecting its precipitation and impact
228 range during the Meiyu period (Zhao et al., 2010). Figure 4a shows a positive
229 correlation between the maximum intensity and the maximum radius of cyclone
230 development. The stronger the intensity of a cyclone is, the larger its radius. Therefore,
231 the horizontal scale of most strong cyclones is larger than that of weak cyclones, the
232 precipitation is greater, and the precipitation range is larger. From the distribution of

233 difference value of track step between the maximum intensity and the radius of the
 234 cyclone shown in Figure 4b, the number of cyclones that reach both at the same time
 235 accounts for 45% of the total number of cyclones. Of the remaining Jianghuai cyclones,
 236 more reach the maximum intensity first and continue to develop to the maximum
 237 horizontal scale.

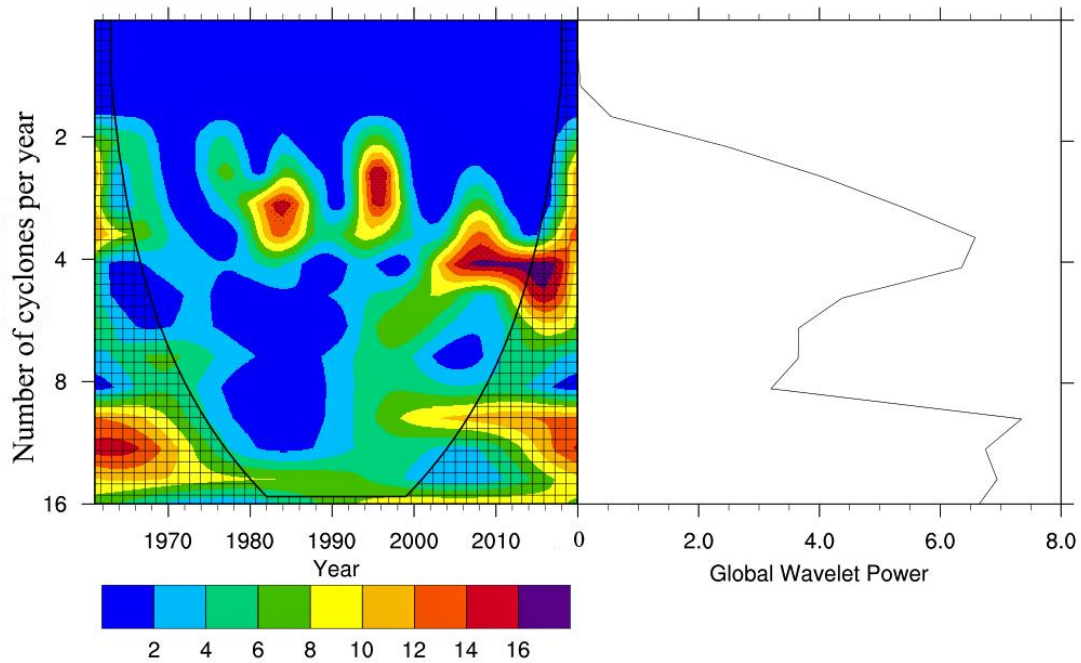


238 Fig 3. Distributions of the number of selected cyclones versus their (a) intensities (units:
 239 10^{-5} s^{-1}), (b) radii (units: km), and (c) lifetimes (units: days).



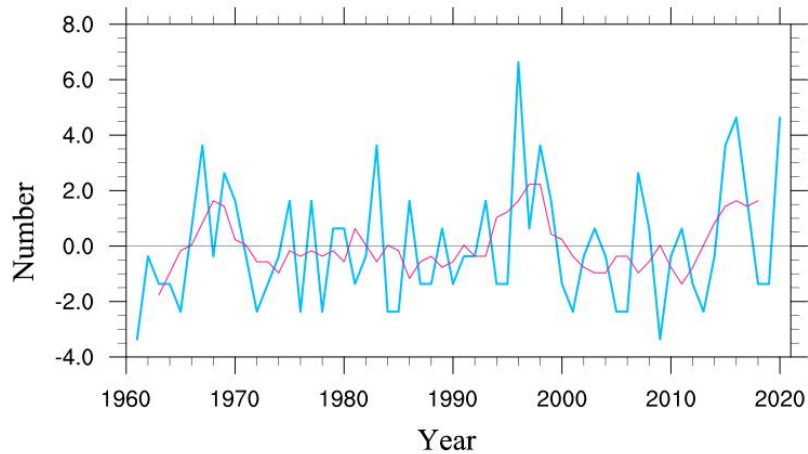
240 Fig 4. Correlation between maximum intensity (units: 10^{-5} s^{-1}) and maximum radius
 241 (units: km) (a) and their difference value of track step during the development of the
 242 Jianghuai cyclone in the Meiyu period (b).

243 The frequency of Jianghuai cyclone occurrence refers to the total number of
 244 cyclones is characterized by multiperiod variation (Figure 5). The shaded area in the
 245 figure indicates that the 95% confidence interval according to the T test is passed.
 246 Strong 2–4-year quasiperiodic variation is observed for 1980-1990 and 1990-2000.
 247 After 2000, the quasiperiodic change in cyclones is approximately 4-5 years. This
 248 change period corresponds to the period of abnormal change in Meiyu. Chen et al.
 249 (2019) pointed out that 3~4 years of quasiperiodic change is the main component of
 250 abnormal changes in Meiyu when studying the quasiperiodic change in Meiyu. This
 251 quasiperiodic variation component is mainly influenced by the out-of-ocean forcing of
 252 the Indian Ocean dipole (IOP), which changes from the ENSO in the previous winter
 253 to late spring and early summer with seasonal changes (Liang et al., 2018). During the
 254 positive phase of the IOP, the strong warming of the Indian Ocean triggers a strong
 255 Indian monsoon. This leads to a strengthening of the WPSH and an increase in
 256 precipitation in southern China. The southwestern rapids, which are enhanced by the
 257 positive IOP, also provide sufficient water vapor and warm advection to generate
 258 favorable conditions for the development of the Jianghuai cyclone.



259 Fig 5. Periodic wavelet analysis diagram of Jianghuai cyclones during the Meiyu period
 260 from 1961 to 2020 (units: year) (shadow indicates passing the 95% confidence interval
 261 according to the T test).

262 Jianghuai cyclones are not only characterized by multiperiod variability but also
 263 have significant interdecadal variability. Figure 5 shows the activity frequency anomaly
 264 and 5-year sliding average of cyclones during the Meiyu period from 1961 to 2020. The
 265 frequency of cyclone activity was the highest in 1996 and the lowest in 1961 and 2009.
 266 In the long term, the frequency of cyclone activity in the middle and lower reaches of
 267 the Yangtze River increased in 1965-1970, in 1990-2000 and after 2010. It decreased
 268 in 1970-1990 and 2000-2010. The interdecadal variability trend of Jianghuai cyclones
 269 is similar to the interdecadal variability trend of precipitation during the Meiyu period
 270 (Chen et al., 2019).



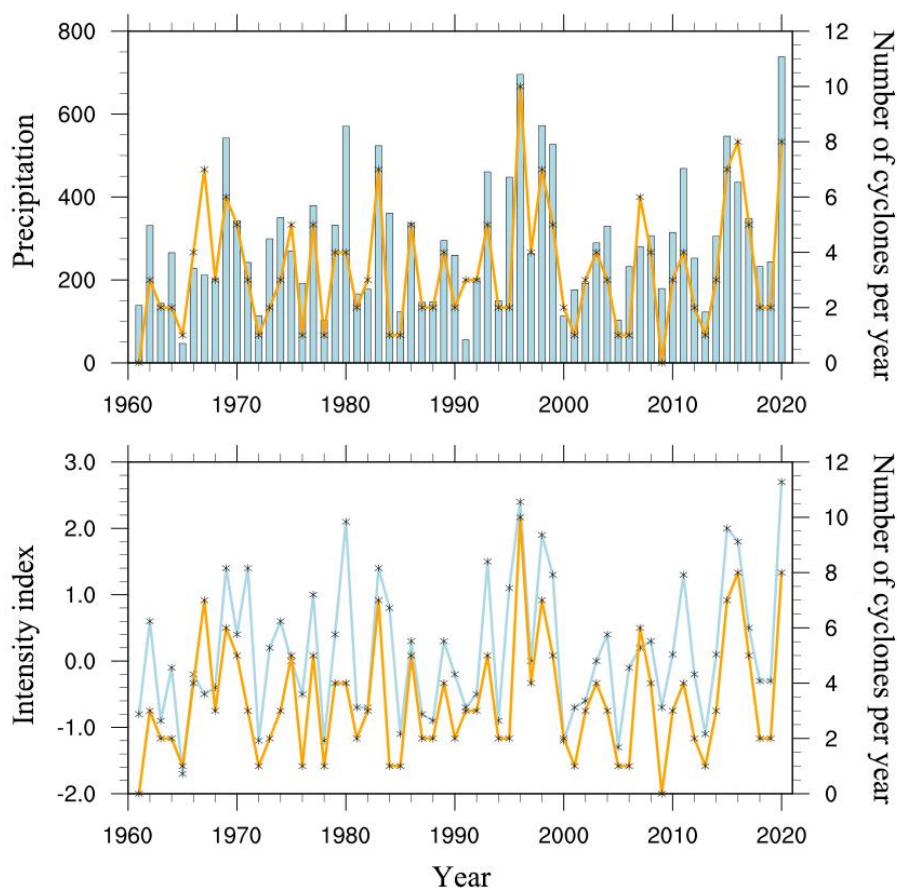
271 Fig 6. Frequency anomaly and 5-year sliding average of cyclones. The blue line shows
 272 the anomalies in the number of cyclones, and the pink line shows the 5-year sliding
 273 average of the anomalies.

274 **3.2 Linkage between cyclone activity and concurrent rainfall in the middle and**
 275 **lower reaches of the Yangtze River.**

276 The Jianghuai cyclones are mainly active in the middle and lower reaches of the
 277 Yangtze River (Huang et al., 2019; Li et al., 2002). Under the influence of the
 278 strengthening westward extension of the WPSH during the Meiyu period, the Jianghuai
 279 cyclones are restricted from entering the sea to some extent (Qin et al., 2015; Wu et al.,
 280 2020). They form rainstorms and gales in the middle and lower reaches of the Yangtze
 281 River and the coastal areas. A large part of the precipitation in the Meiyu period comes
 282 from cyclone precipitation (Zhang et al., 2018). The intensity of Meiyu is usually
 283 expressed by the Meiyu intensity index. The intensity of precipitation is affected not
 284 only by precipitation but also by the number of precipitation days in the Meiyu period.
 285 Both jointly determine the intensity of Meiyu in that year.

286 The time-series plots of the number of cyclones related to precipitation and the
 287 intensity index during the Meiyu period from 1961 to 2020 are given in Figure 6a and
 288 6b. We found that the number of cyclones has a positive correlation coefficient of 0.769
 289 with precipitation in the Meiyu period passing the 99% confidence interval according
 290 to the T test. The number of cyclones was also positively correlated with the Meiyu

291 intensity index, with a correlation index of 0.760 passing the 99% confidence interval
 292 according to the T test. The frequency of Jianghuai cyclone activity in years with a
 293 strong Meiyu index is high; the frequency of Jianghuai cyclone activity in years with a
 294 weak Meiyu index is low.



295 Fig 7. (a) Changes in precipitation (blue bar chart) (unit: mm/day) and the number of
 296 cyclones (orange line); (b) intensity index (blue line) and the number of cyclones
 297 (orange line) in the Meiyu period from 1961 to 2020.

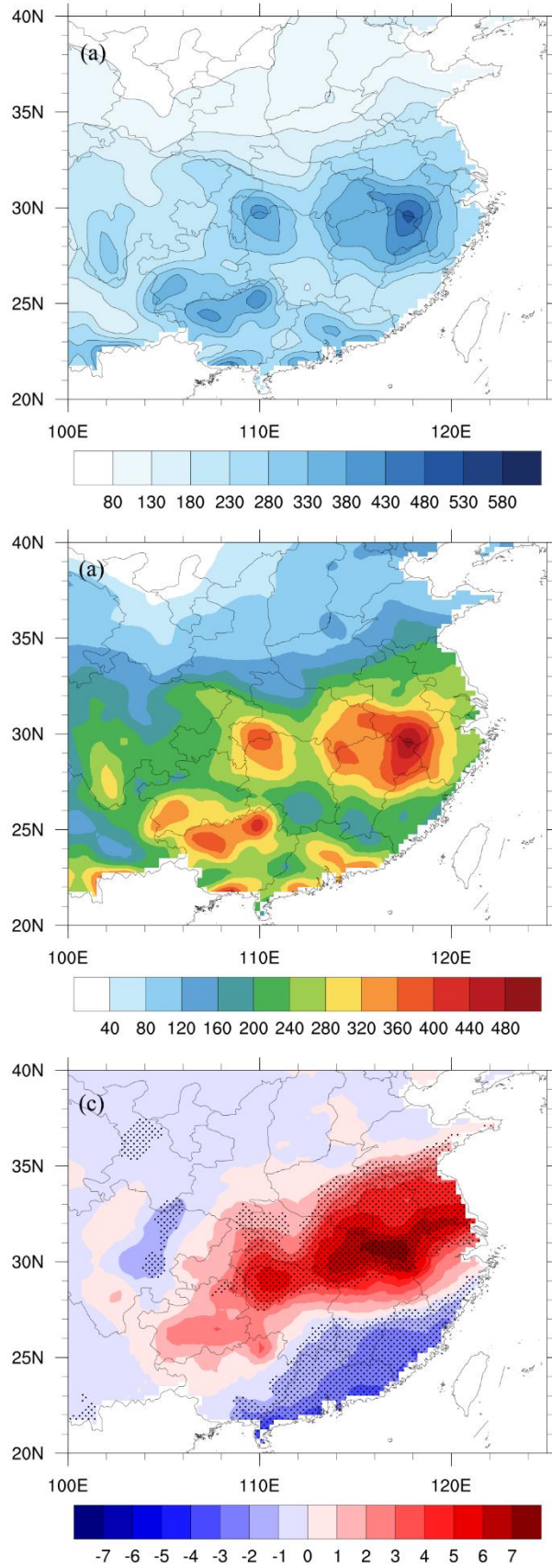
298 Figure 8a shows the spatial distribution of annual average precipitation during the
 299 Meiyu period from 1961 to 2020. The areas with large precipitation values in the middle
 300 and lower reaches of the Yangtze River are mainly located in the Dabie Mountains of
 301 Anhui Province, the northern part of Jiangxi Province, the eastern part of Hubei
 302 Province and the western part of Hubei Province. The maximum annual average
 303 precipitation during the Meiyu period in southern Anhui can even exceed 480 mm. The

304 occurrence of large precipitation areas during the Meiyu period is closely related to the
305 topography of the region (Wu et al., 2023).

306 If precipitation and Jianghuai cyclone activity existed on the same day during the
307 Meiyu period, we defined that day as a Jianghuai cyclone precipitation day. The
308 remaining days in the Meiyu period were treated as non-Jianghuai cyclone precipitation
309 days. Figure 8b shows the spatial distribution of the proportion of cyclone precipitation
310 relative to total precipitation during the Meiyu period. As shown in the figure, the main
311 areas affected by cyclone precipitation are the middle and lower reaches of the Yangtze
312 River. The Huaihe River basin in northern Anhui Province is the most affected area.
313 The cyclone precipitation in the Huaihe River basin accounts for more than 47% of the
314 total precipitation during the Meiyu period, while the cyclone-influenced precipitation
315 in other areas accounts for more than 35% of the total precipitation. In general, the
316 degree of cyclone-influenced precipitation in the middle and lower reaches of the
317 Yangtze River shows an east–west band distribution and a gradual decrease from
318 coastal to inland areas. This indicates that the distribution of the large-value area and
319 the characteristics of the band distribution are related to the northeast and eastward
320 tracks of the Jianghuai cyclone. Its precipitation capacity gradually increases with the
321 development of cyclone movement.

322 Figure 8c shows the spatial distribution of the daily mean precipitation anomaly
323 of the Jianghuai cyclone. The shaded part indicates that the 95% confidence interval is
324 passed according to the T test. The anomaly is based on the whole Meiyu period from
325 1961 to 2020 (The exceptions mentioned below are also based on the whole Meiyu
326 period from 1961 to 2020). When the Jianghuai cyclone is active, the middle and
327 lower reaches of the Yangtze River to the east of 108°E show an abnormal increase in
328 precipitation. However, Fujian, Guangdong and other places show an abnormal
329 decrease. Among them, the maximum value of abnormally increased precipitation can
330 exceed 7 mm/day in areas such as southern Anhui, eastern Hubei and northern Jiangxi.
331 The large-value areas of precipitation anomalies are consistent with the large-value
332 areas of cyclone occurrence frequency sources. It is inferred that the spatial distribution

333 of precipitation anomalies has a connection with the distribution of cyclone genesis
334 locations. This phenomenon of increasing and decreasing precipitation anomalies is
335 bounded by approximately 27°N and distributed north–south in the form of dipoles.



336 Fig 8. (a) Annual mean precipitation during the Meiyu period from 1961 to 2020 (units:

337 mm/year); (b) proportion of Jianghuai cyclone precipitation relative to total
338 precipitation during the Meiyu period (units: %); (c) daily mean precipitation anomaly
339 of the Jianghuai cyclone during the Meiyu period (units: mm/day) (shadow indicates
340 passing the 95% confidence interval according to the T test).

341 Figure 9 shows the evolution of composite geopotential height and horizontal wind
342 anomalies for three different levels of Jianghuai cyclones from day -4 to +2 during the
343 Meiyu period. Composite geopotential height anomalies are significant at the 95%
344 confidence level based on a T test. Vectors are plotted if wind anomalies are significant
345 at the 95% confidence level based on a T test in at least one direction.

346 Day 0 is the day on which the cyclone first appears in the specified area. Most
347 areas of the lower and middle troposphere (700 hPa, 850 hPa) in the middle and lower
348 Yangtze River on day 0 are covered by significant negative geopotential height
349 anomalies with peak magnitudes greater than -11 gpm. There is a significant positive
350 geopotential height anomaly with a peak magnitude of over 13 gpm on the southeast
351 side of the negative geopotential height anomaly. These anomalies form meridional
352 dipole structures in the middle and lower troposphere geopotential height field. The
353 southwest wind anomaly is significant in the middle and lower reaches of the Yangtze
354 River. The south of Anhui Province and the north of Jiangxi Province are between the
355 positive geopotential height anomaly and negative geopotential height anomaly. The
356 existence of these anomalies indicates the enhancement of southwest rapids and the
357 strengthening of the WPSH. The negative geopotential height anomalies at 500 hPa
358 height on day 0 are mainly in Mongolia, Shanxi and other places. Strong southwest
359 wind anomalies exist between the positive and negative geopotential height anomalies.
360 The negative geopotential height anomalies in the Mongolian region exceed -7 gpm.

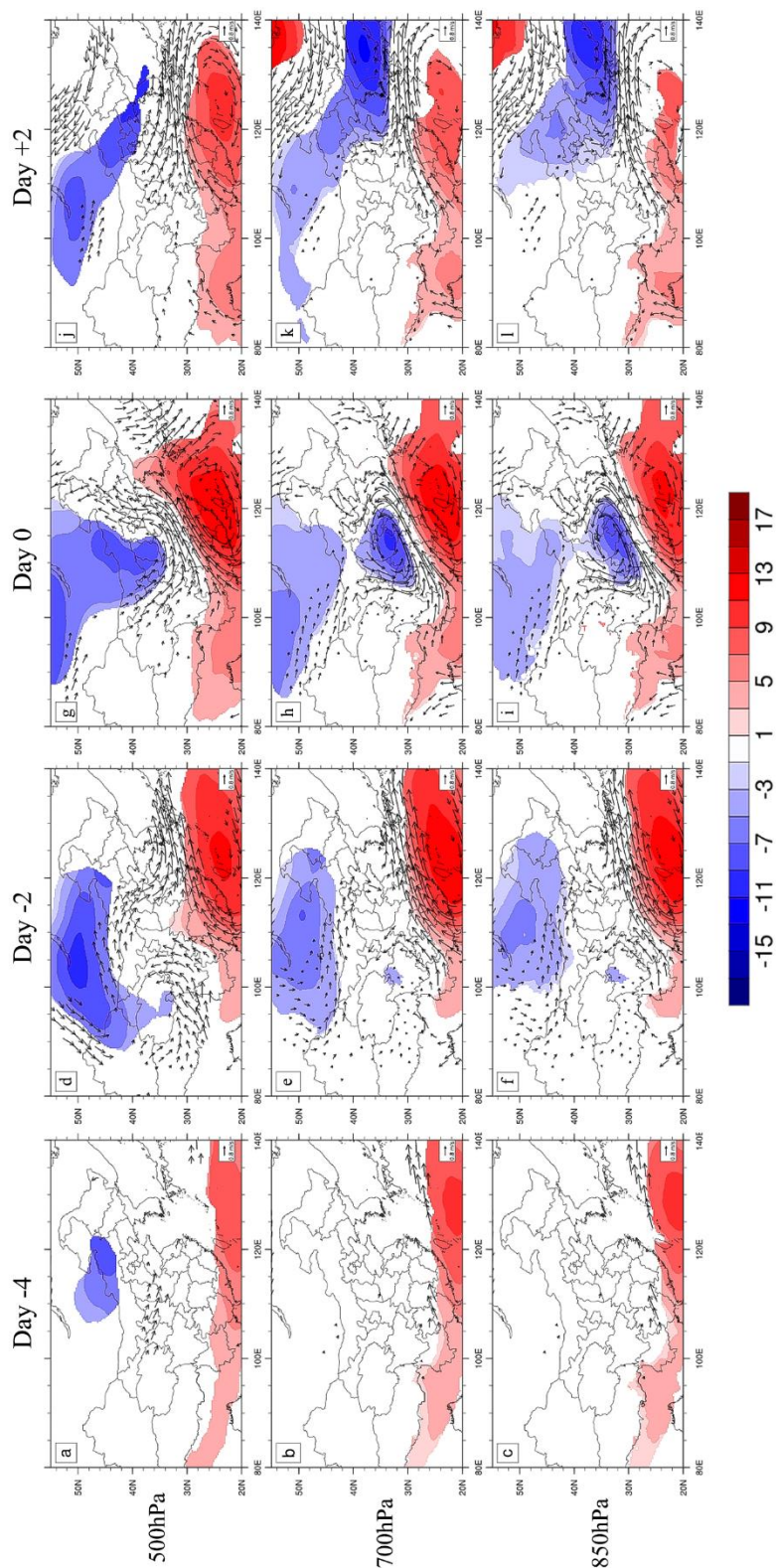
361 The negative geopotential height anomalies on all three isobaric surfaces can be
362 traced back to Mongolia, Inner Mongolia and part of Northeast China on day -2.
363 Negative geopotential height anomalies at 500 hPa can be traced to day -4. On day -4,
364 significant southwestern wind anomalies exist in southwestern Hunan at 700 hPa and

365 850 hPa. Significant northwest wind anomalies exist in the Yellow River basin of China
366 at 500 hPa. By day -2, the negative geopotential height anomalies in Mongolia, Inner
367 Mongolia and some northeastern areas are enhanced for all three isobars. The positive
368 geopotential height anomalies of the WPSH are enhanced and extend northward to the
369 southern part of the middle and lower reaches of the Yangtze River. There are
370 significant southwest wind anomalies at the three isobaric surfaces in the south of the
371 middle and lower reaches of the Yangtze River, while there are significant northwest
372 wind anomalies at 500 hPa in the north of Anhui Province and Jiangsu Province. The
373 negative geopotential height anomalies on the three isobaric surfaces move eastward
374 with the formation and development of Jianghuai cyclones. On day +2, the lower
375 reaches of the Yangtze River are mainly affected by the combined action of anomalous
376 southwest winds and northwest winds. The positive geopotential height anomaly of the
377 WPSH is weakened.

378 Therefore, the abnormal precipitation caused by the Jianghuai cyclone mainly
379 comes from the abnormal southwest winds and the strengthening of the WPSH. The
380 enhanced southwest jet provides sufficient warm and moist air for the formation of
381 cyclones and promotes the eastward migration of cyclones after formation. Liu et al.
382 (2020) and Zhao et al. (2021) studied the causes of the super strong Meiyu year in 2020,
383 mentioned that the WPSH is unusually strong and westward accompanied by an
384 abnormal increase in precipitation. Liu et al. (2020) found that the enhanced southwest
385 jet stream is conducive to the development of vertical movement in the middle and low
386 levels, which provides the necessary dynamic conditions for the formation of sustained
387 precipitation during the Meiyu in 2020.

388 Cold air activity is one of the important factors for the formation of heavy
389 precipitation, which can promote the convergence and uplift of low level necessary for
390 heavy precipitation (Liu et al., 2020). The enhanced negative geopotential anomaly
391 over Mongolia provides cold and dry air brought by the westerly jet for cyclone
392 development. The increasing frequency of cyclones over the Yangtze River and Huaihe
393 River leads to the abnormal increase in precipitation in the middle and lower reaches of

394 the Yangtze River during the Meiyu period. However, due to the strengthening of the
 395 WPSH, the southern part of China is controlled by the abnormal positive geopotential
 396 height, and the precipitation decreases. Zhao et al. (2021) also found that when the
 397 WPSH enhanced, there was a decrease in precipitation in South China.



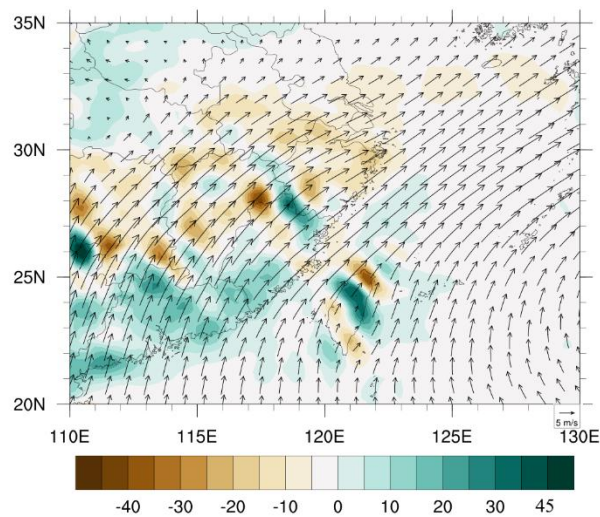
398 Fig 9. Evolution of composite geopotential height anomalies (shading; units: gpm) and
399 horizontal wind anomalies (units: m/s) on the 850 hPa, 700 hPa, and 500 hPa isobaric
400 surfaces for day -4 (a-c), day -2 (d-f), day 0 (g-i) and day +2 (j-l) for the 202 selected
401 Jianghuai cyclones. Shading indicates that composite geopotential height anomalies are
402 significant at the 95% confidence level based on a T test. Vectors are plotted if wind
403 anomalies are significant at the 95% confidence level based on a T test in at least one
404 direction.

405 Figure 10 shows the climatic distribution of water vapor flux and water vapor flux
406 divergence at a pressure level of 850 hPa during the Meiyu period. The water vapor
407 involved in the precipitation process of the Jianghuai cyclone during the Meiyu period
408 mainly comes from the water vapor brought by the southwest jet of the summer
409 monsoon in the low-latitude area. During Jianghuai cyclone development, the middle
410 and lower reaches of the Yangtze River are mostly in the water vapor convergence area,
411 which is conducive to the generation of precipitation (Chen et al., 2020).

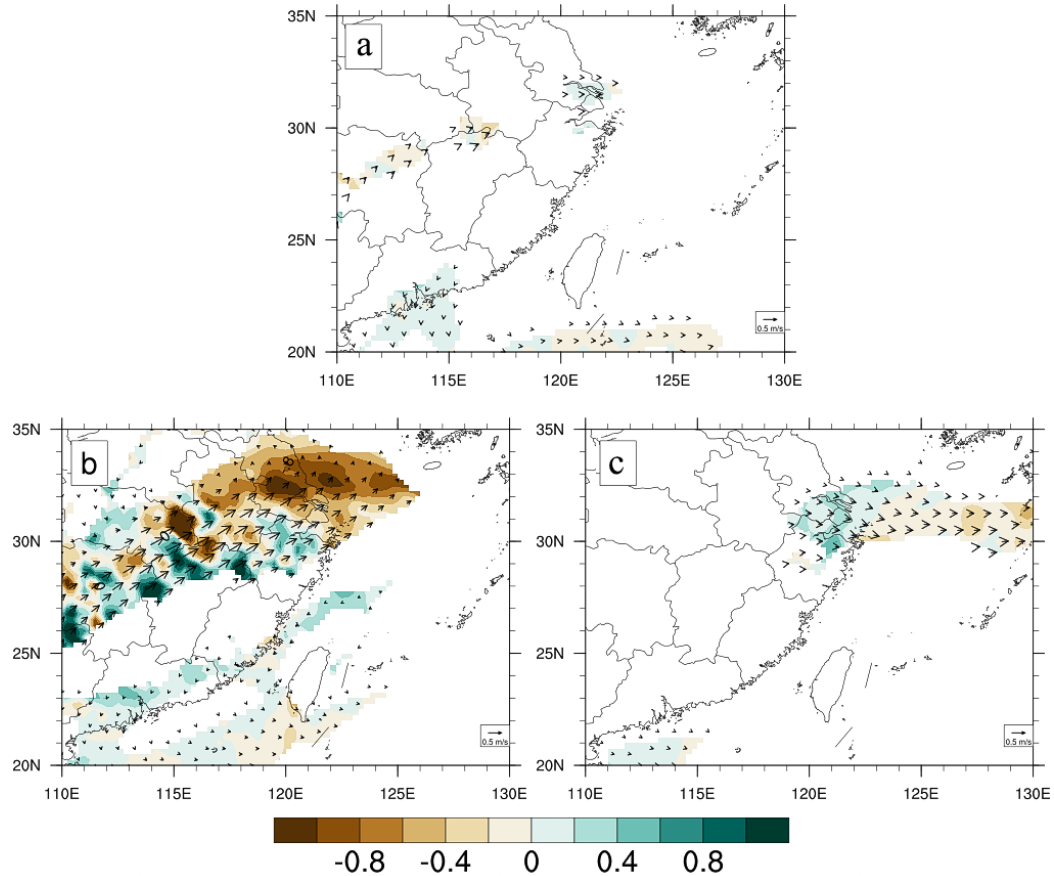
412 Figure 11 shows the distribution of water vapor flux anomalies and water vapor
413 flux divergence anomalies at the pressure level of 850 hPa during the Jianghuai cyclone
414 from day -2 to day +2. The color field and wind vector arrows in the figure both passed
415 the 95% significance according to the T test. On day -2, a significant water vapor
416 convergence anomaly and water vapor transport in the southwest direction appear in
417 southern Anhui Province. The anomalies of water vapor flux and water vapor flux
418 dispersion are mainly concentrated on day 0. There is significant anomalous water
419 vapor convergence up to $-1 \text{ g}\cdot\text{cm}^{-2}\cdot\text{hPa}^{-1}$ in eastern Hubei Province, Anhui Province and
420 Jiangsu Province on day 0. Anomalous water vapor dispersion exists in the southern
421 part of the middle and lower reaches of the Yangtze River and some areas in southern
422 China. On day +2, with the development of the cyclone's eastward movement, only the
423 southern part of Jiangsu Province and the northern part of Zhejiang Province have
424 abnormal water vapor flux in the eastward direction. The precipitation in the area begins
425 to gradually weaken at this time.

426 From day -2 to day 0, the abnormal water vapor flux and water vapor flux
427 divergence configuration make the warm and wet air in the low-latitude area transport
428 to the middle and lower reaches of the Yangtze River. The abnormal water vapor flux
429 has a negative value, water vapor convergence occurs, local water vapor volume
430 increases, and finally, the precipitation in the region increases. Liu et al. (2020) studied
431 the strong rainfall in 2020, they found that there was an enhanced water vapor transport,
432 and the repeated occurrence of convergence movement. Both of them caused the
433 precipitation time to increase in the Jianghuai River basin.

434 In contrast, the anomaly of water vapor flux in southern Guangdong and other
435 regions is divergent. This leads to a decrease in local water vapor volume and
436 precipitation in this region. These results indicate that the variations in water vapor flux
437 and divergence related to cyclones are mainly from warm and wet air transported from
438 low latitudes to the middle and lower reaches of the Yangtze River. Therefore, there is
439 a positive correlation between cyclone activity and precipitation in the middle and
440 lower reaches of the Yangtze River.



441 Fig 10. Distribution of 850 hPa daily mean water vapor flux (unit: $\text{g}\cdot\text{cm}^{-2}\cdot\text{hPa}^{-1}$) and
442 water vapor flux divergence (unit: $10^{-8}\text{ g}\cdot\text{cm}^{-2}\cdot\text{hPa}^{-1}\cdot\text{s}^{-1}$) of cyclones over the Yangtze
443 and Huaihe rivers during 1961-2020 (color diagram shows water vapor flux divergence,
444 and vector diagram shows water vapor flux).



445 Fig 11. Distribution of the 850 hPa daily mean water vapor flux anomaly (unit: $\text{g}\cdot\text{cm}^{-2}\cdot\text{hPa}^{-1}$) and water vapor flux divergence anomaly (unit: $10^{-8}\text{ g}\cdot\text{cm}^{-2}\cdot\text{hPa}^{-1}\cdot\text{s}^{-1}$) of
 446 cyclones over the Yangtze and Huaihe rivers during 1961-2020 (color diagram shows
 447 water vapor flux divergence, and vector diagram shows water vapor flux). The colored
 448 region passed the 95% confidence interval according to a T test. If the vapor flux
 449 anomaly is significant at the 95% confidence level for the T test in at least one direction
 450 (zonal or meridian), the vector is plotted.
 451

452 4. Summary and discussion

453 Based on ERA5 reanalysis of sea level pressure data and using the relative
 454 vorticity method to identify and track cyclones, we have examined the impacts of the
 455 climatological characteristics of Jianghuai cyclones. The linkages between cyclone
 456 activity and precipitation in the middle and lower reaches of the Yangtze River during
 457 the Meiyu period are also analyzed.

458 During the Meiyu period, Jianghuai cyclones are mainly generated at the junction
459 of western Hubei and Chongqing Municipality, eastern Hubei Province, northern
460 Jiangxi Province, central and southern Anhui Province, and Jiangsu and Zhejiang
461 provinces. These cyclones develop and move to the sea in the east or northeast direction.
462 There is a positive correlation between the maximum intensity and maximum radius of
463 Jianghuai cyclones. The higher the cyclone intensity is, the larger the radius will be. Its
464 occurrence frequency not only has the characteristics of multicycle variation but also
465 has obvious interdecadal variation, which has a good correspondence with the periodic
466 and interdecadal variation in precipitation in the Meiyu period.

467 There is a positive correlation between the frequency of cyclone activity and
468 precipitation in the Meiyu period. The frequency of Jianghuai cyclone activity is high
469 in the years with strong Meiyu rainfall and low in the years with weak Meiyu rainfall.
470 The percentage of precipitation affected by Jianghuai cyclone activity in the middle and
471 lower reaches of the Yangtze River can reach up to 47%. The spatial distribution is in
472 the shape of an east–west belt, and the degree of influence gradually decreases from the
473 coast to the interior. When the Jianghuai cyclone is active, the precipitation increases
474 abnormally in the middle and lower reaches of the Yangtze River east of 108°E.
475 Precipitation decreases abnormally in Fujian Province and Guangdong Province. The
476 spatial distribution of precipitation anomalies is related to the genesis locations of
477 cyclone frequency, and the positive and negative anomalies are distributed north–south
478 in the form of dipoles based on the latitude line at approximately 27°N as the boundary.

479 The geopotential height anomaly field and the horizontal wind vector anomaly
480 field of the Jianghuai cyclones during the Meiyu period are synthesized and analyzed.
481 There is an enhanced positive geopotential height anomaly of the WPSH during cyclone
482 activity. The negative geopotential altitude anomaly of Mongolia and the abnormal
483 southwest jet are enhanced. All of these factors lead to an increase in precipitation in
484 the middle and lower reaches of the Yangtze River. The abnormal leading signal of the
485 negative geopotential height in Mongolia can be traced to day -2 of the cyclone activity,
486 and the signal can be traced to day -4 at 500 hPa. From day -2 to day 0 of cyclone

487 activity, the abnormal distribution of water vapor flux and water vapor flux divergence
488 cause the warm and wet air at the low latitudes to be transported to the middle and lower
489 reaches of the Yangtze River. They promote the generation and development of
490 cyclones and increase precipitation in the middle and lower reaches of the Yangtze
491 River.

492 We explored the cyclone characteristics and study emphasizes the link between
493 cyclone activity and Yangtze River precipitation. Spatially, abnormal precipitation
494 patterns are identified, tracing the evolution of geopotential height anomalies and water
495 vapor flux. But the specific mechanism by which the southwest jet affects cyclones
496 during the Meiyu period is not clear enough. Zhang et al. (2018) suggest that the
497 strengthening of the Southwest jet will lead to the development of α mesoscale low-
498 pressure disturbance near the Meiyu Front and the occurrence of extreme precipitation.
499 Liu et al. (2020) found that the strengthening of the southwest jet made the southerly
500 meridional strong gradient zone on the north side of the meridional wind maximum
501 center move northward in the low-level dynamic conditions of the rainstorm process
502 during Meiyu. How the Southwest jet stream influences the development of physical
503 factors to promote the formation of Jianghuai cyclones remains to be considered and
504 analyzed. Zhao et al. (2010) found that the causes of Jianghuai cyclones with different
505 intensities were different through a case study. Therefore, we think it is also necessary
506 to consider the difference in the influence of different intensities of Jianghuai cyclones
507 on precipitation. These problems need further analysis and research.

508 **Competing interests**

509 The contact author has declared that none of the authors has any competing interests.

510 **References**

- 511 Bao, Y, Y.: Similarities and Differences of Monsoon Circulations between 2016 and
512 1998 Meiyu Periods in Middle and Lower Reaches of the Yangtze River and
513 Comparison of Their Physical Mechanisms. Chinese Journal of Atmospheric
514 Sciences., 45, 994–1006, 2021. DOI: [10.3878/j.issn.1006-9895.2101.20174](https://doi.org/10.3878/j.issn.1006-9895.2101.20174)
- 515 Cai, Y, X., He, H., Lu, H., Zhu, L, Y., and Lu, Q, Q.: Synoptic and climatic
516 characteristics of persistent rainstorm in Guangxi in June 2020. Journal of
517 Meteorological Research and Application., 4, 113-117, 2021.
518 DOI:[10.19849/j.cnki.CN45-1356/P.2021.1.20](https://doi.org/10.19849/j.cnki.CN45-1356/P.2021.1.20).
- 519 Chen, L, J., Zhao, J, H., Gu, W., Liang, P., Zhi, R., Peng, J, B., Zhao, S, Y., Gao, H., Li,
520 X. and Zhang, P, Q.: Advances of Research and Application on Major Rainy Seasons
521 in China. Journal Of Applied Meteorological Science., 30, 385-400, 2019.
522 DOI: [10.11898/1001-7313.20190401](https://doi.org/10.11898/1001-7313.20190401)
- 523 Chen, T., Zhang, F, H., Yu, C., Ma, J., Zhang, X, D., Shen, X, L., Zhang, F. and Luo,
524 Q.: Synoptic analysis of extreme Meiyu precipitation over Yangtze River Basin during
525 June-July. Meteor Mon., 46, 1415-1426, 2020.
526 DOI: [10.7519/j.issn.1000-0526.2020.11.003](https://doi.org/10.7519/j.issn.1000-0526.2020.11.003)
- 527 Ding, Y, H.: Summer monsoon rainfalls in China. J Meteor Soc Jpn.,70, 373-396, 1992.
528 DOI: https://doi.org/10.2151/jmsj1965.70.1B_373
- 529 Ding, Y, H.: Seasonal march of the east-Asian summer monsoon. Chang C P. East Asian
530 Monsoon. Hackensack: World Scientific., 64, 2004.
531 DOI: https://doi.org/10.1142/9789812701411_0001
- 532 Ding, Y, H., Liu, J, J., Sun, Y., Liu, Y, J., He, J, H., Song, Y, F.: A Study of the Synoptic-
533 Climatology of the Meiyu System in East Asia. China J Atmos Sci., 31, 1082-1101,
534 2007. DOI: <https://d.wanfangdata.com.cn/periodical/daqikx200706006>
- 535 GB/T 33671-2017, Meiyu monitoring indices.
536 DOI:http://fj.cma.gov.cn/zfxxgk/zwgk/flfgbz/dfbz/202209/t20220921_5098384.htm
537 1
- 538 He, L, F., Chen, T., Zhou, Q, L. and Li, Z, C.: The Meso-β Scale Convective System of

539 a Heavy Rain Event on July 10, 2004 in Beijing. Journal Of Applied Meteorological
540 Science., 18, 655-665, 2007. DOI: [10.3969/j.issn.1001-7313.2007.05.010](https://doi.org/10.3969/j.issn.1001-7313.2007.05.010)

541 Hersbach, H., and Coauthors.: ERA5 hourly data on pressure levels from 1940 to
542 present. Copernicus Climate Change Service (C3S) Climate Data Store (CDS)., 2018.
543 DOI: [10.24381/cds.bd0915c6](https://doi.org/10.24381/cds.bd0915c6)

544 Hodges, K. I.: A general method for tracking analysis and its application to
545 meteorological data. Monthly Weather Review., 122, 2573-2586, 1994.
546 DOI:[https://doi.org/10.1175/1520-0493\(1994\)122<2573:AGMFTA>2.0.CO;2](https://doi.org/10.1175/1520-0493(1994)122<2573:AGMFTA>2.0.CO;2).

547 Hodges, K, I.: Feature tracking on the unit sphere. Monthly Weather Review., 123,
548 3458-3465, 1995.
549 DOI:[https://doi.org/10.1175/1520-0493\(1995\)123<3458:FTOTUS>2.0.CO;2](https://doi.org/10.1175/1520-0493(1995)123<3458:FTOTUS>2.0.CO;2).

550 Huang, W, Y., Sun, Y., Lu, C, H., Yao, L, N. and Dong, Q.: Statical analysis of Jianghuai
551 cyclone causing Jianguo regional heavy rain in summer nearly 40 years. Meteor Mon.,
552 45, 843-853, 2019. DOI: [10.7519/j.issn.1000-0526.2019.06.010](https://doi.org/10.7519/j.issn.1000-0526.2019.06.010)

553 Jiang, L, Z., Fu, S, M., Sun, J, H.: New method for detecting extratropical cyclones: the
554 eight-section slope detecting method. Atmospheric and Oceanic Science Letters, 13,
555 436-442, 2020.
556 DOI:[10.1080/16742834.2020.1754124](https://doi.org/10.1080/16742834.2020.1754124).

557 Jiangsu Provincial Weather Bureau: Jiangsu Province Weather Forecast Techniacal
558 Manual. Beijing: China Meteorological Press., 22-33, 2017.

559 Li, B., Yu, W, P., Lu, Y. and Lu, D, C.: The numerical simulating study of the mesoscale
560 characteristics on development of Jianghuai cyclones. Science meteorologic., 22, 72-
561 80, 2002. DOI: [10.3969/j.issn.1009-0827.2002.01.009](https://doi.org/10.3969/j.issn.1009-0827.2002.01.009).

562 Liang, P., Chen, L, J., Ding, Y, H., He, J, H. and Zhou, B.: Relationship between long-
563 term variability of Meiyu over the Yangtze River and ocean and Meiyu's
564 predictability study. Acta Meteorologica Sinica., 76, 379-393, 2018.
565 DOI:[10.11676/qxxb2018.009](https://doi.org/10.11676/qxxb2018.009).

566 Liu, Y, Y., Ding, Y, H.: Characteristics and possible causes for extreme Meiyu in 2020.
567 Meteor Mon.,46, 1393-1404, 2020. DOI: [10.7519/j.issn.1000-0526.2020.11.001](https://doi.org/10.7519/j.issn.1000-0526.2020.11.001)

568 Lu, C, H.: A Modified Algorithm for Identifying and Tracking Extratropical Cyclones.
569 Advances in atmospheric sciences., 34, 909-924, 2017.DOI: [10.1007/s00376-017-](https://doi.org/10.1007/s00376-017-6231-2)
570 [6231-2](https://doi.org/10.1007/s00376-017-6231-2)

571 Pascal, J, Mailier., David, B, Stephenson., Christopher, A, T, Ferro.: Serial Clustering
572 of Extratropical Cyclones. Monthly weather review, 134, 2224-2240, 2006.

573 Ninomiya, K., Murakami, T.: The early summer rainy season (Baiu) over Japan.
574 Monsoon Meteorology., New York: Oxford University Press, 93-121, 1987.

575 Oh, T, H., Kwon, W, T., Ryoo, S, B.: Review of the researches on Changma and future
576 observational study. Adv Atmos Sci, 14, 207-222, 1997.

577 Pang, Y., Wang, L, J. and Yu, B.: The relationship between 10-30d low frequency
578 oscillation and the rainfall over Changjiang-Huaihe River valley during Meiyu
579 period. Trans Atmos Sci., 36, 742-750, 2013.
580 DOI: [10.3969/j.issn.1674-7097.2013.06.011](https://doi.org/10.3969/j.issn.1674-7097.2013.06.011)

581 Qian, W, H., Lee, D, K.: Seasonal march of Asian summer monsoon. Int J Climatol.,
582 20, 1371-1386, 2000.
583 DOI: [10.1002/1097-0088\(200009\)20:11<1371::AID-JOC538>3.0.CO;2-V](https://doi.org/10.1002/1097-0088(200009)20:11<1371::AID-JOC538>3.0.CO;2-V)

584 Qin, T., Wei, L, X.: The statistic and variance of cyclones entering coastal waters of
585 china in 1979-2012. Acta Oceanologica Sinica., 2015.
586 DOI: [10.3969/j.issn.0253-4193.2015.01.005](https://doi.org/10.3969/j.issn.0253-4193.2015.01.005)

587 Saito, N.: Quasi-stationary waves in mid-latitudes and Baiu in Japan. J Meteor Soc, 63,
588 983-995, 1995.

589 Shen, Y., Sun, Y., Cai, N, H., Su, X. and Shi, D, W.: Analysis on the generation and
590 evolution of a Jianghuai Cyclone responsible for extreme precipitation event. Meteor
591 Mon.,45, 166-179, 2019. DOI: [10.7519/j.issn.1000-0526.2019.02.003](https://doi.org/10.7519/j.issn.1000-0526.2019.02.003)

592 Simmonds, I., Keay, K.: Mean Southern Hemisphere extratropical cyclone behavior in
593 the 40-year NCEP-NCAR reanalysis. J Climate., 13, 873-885, 2000.
594 DOI: [10.1175/1520-0442\(2000\)013<0873:MSHECB>2.0.CO;2](https://doi.org/10.1175/1520-0442(2000)013<0873:MSHECB>2.0.CO;2)

595 Simmonds, I., Murray, R, J.: Southern extratropical cyclone behavior in ECMWF
596 analyses during the FROST special observing periods. *Weather& Fore-casting.*, 14,
597 878-891, 1999.
598 DOI:[10.1175/1520-0434\(1999\)014<0878:SECBIE>2.0.CO;2](https://doi.org/10.1175/1520-0434(1999)014<0878:SECBIE>2.0.CO;2)

599 Su, X., Kang, Z, M., Zhuang, X, R. and Chen, S, J.: Uncertainty analysis of heavy rain
600 belt forecast during the 2020 Meiyu period. *Meteor Mon.*, 47, 1336-1346, 2021. DOI:
601 [10.7519/j.issn.1000-0526.2021.11.003](https://doi.org/10.7519/j.issn.1000-0526.2021.11.003).

602 Tao, S, Y., Ding, Y, H. and Zhou, X, P.: Study on heavy rain and severe convective
603 weather. *Chinese Journal of Atmospheric Sciences.*1979.

604 Wang, J, H., Niu, D., Ren, S, Y., Miao, C, S. and Song, P.: Comparative Study On
605 Development Of Different Deep Jianghuai Rivers Cyclones Entering the Sea and the
606 Influence of Environmental Factors. *Journal Of Tropical Meteorology.*, 31, 744-756,
607 2016. DOI: [10.16032/j.issn.1004-4965.2015.06.003](https://doi.org/10.16032/j.issn.1004-4965.2015.06.003).

608 Wang, Y, L., Wang, L, J.: Characteristics of southern cyclone activity and its influence
609 on precipitation in Yangtze River Basin. *Yangtze River.*, 43, 34-36,68, 2012. DOI:
610 [10.3969/j.issn.1001-4179.2012.09.009](https://doi.org/10.3969/j.issn.1001-4179.2012.09.009).

611 Wang, Y, L., Guan, Z, Y., Jin, D, C. and Ke, D.: Climatic characteristics and interannual
612 variations of cyclones over Changjiang-Huaihe River basin during late spring and
613 early summer from 1980 to 2012. *Trans Atmos Sci.*, 38, 354-361, 2015.
614 DOI: [10.13878/j.cnki.dqkxxb.20130413010](https://doi.org/10.13878/j.cnki.dqkxxb.20130413010)

615 Wang, L, J., Huang, Q, L., Li, Y. and Han, S, R.: Relationship between spatial
616 inhomogeneous distribution of Meiyu rainfall over the Yangtze-Huaihe River Valley
617 and previous SST. *Trans Atmos Sci*, 37, 313-322, 2014. DOI: [10.3969/j.issn.1674-7097.2014.03.008](https://doi.org/10.3969/j.issn.1674-7097.2014.03.008)

618

619 Wei, J, S., Liu, J, Y., Sun, Y. and Xu, Y, C.: Climate characteristics of Jiang-Huai
620 cyclone. *J Meteor Sci*, 33, 196-201, 2013. DOI: [10.3969/2012jms.0112](https://doi.org/10.3969/2012jms.0112)

621 Wernli, H., Schwierz, C.: Surface cyclone in the ERA-40 dataset (1958-2001). Part I:
622 Novel identification method and global climatology. *J Atmos Sci.*, 63, 2486-2507,
623 2006.

624 Wu, J, F., Xu, X, F., Zhao, W, R., Qing, Q. and Zou, L.: Characteristics of Persistent
625 Heavy Rainfall and Water Vapor Transport in Western Sichuan Plateau.
626 Meteorological science and technology., 48, 704-716, 2020.
627 DOI:[10.19517/j.1671-6345.20190301](https://doi.org/10.19517/j.1671-6345.20190301).

628 Wu, Q., Chen, S, J., Bai, Y., Xia, L. and Wang, C, J.: Diagnostic analysis and numerical
629 simulation of a heavy rainstorm associated with the Jianghuai cyclone. Journal of the
630 Meteorological Sciences., 41, 86-98, 2021. DOI: [10.12306/2020jms.0029](https://doi.org/10.12306/2020jms.0029).

631 Wu, Q., Liu, T., Zhang, B., Zhang, Y. and Wang, Y.: A Comparative Analysis of the
632 Heavy Rainstorm Processes of Two Jianghuai Cyclones. Anhui Agri, Sci, Bull., 26,
633 161-171, 2020. DOI: [10.3969/j.issn.1007-7731.2020.09.058](https://doi.org/10.3969/j.issn.1007-7731.2020.09.058)

634 Wu, Q., Feng, J, W., Wang, Y., Chen, Y. and Zhang, L, T.: Spatial and temporal
635 distribution of cyclones over the Jianghuai River during 1979-2018. Meteorology of
636 Shanxi., 06, 15-22, 2021. DOI: [10.3969/j.issn.1006-4354.2020.06.003](https://doi.org/10.3969/j.issn.1006-4354.2020.06.003)

637 Wu, T., Xu, G, Y., Li, S, J. and Wei, F.: Characteristics and Causes of a Mixed-Type
638 Convective Weather During the Formation and Development of a Jianghuai Cyclone
639 in Spring. Advances in Meteorological Science and Technology., 48, 704-716, 2023.
640 DOI:[10.19517/j.1671-6345.20190301](https://doi.org/10.19517/j.1671-6345.20190301).

641 Xu, J., Zhou, C, Y. and Gao, T, C.: Analysis about Development Mechanism of
642 Jianghuai Cyclone in Meiyu Front and Its Relationship with Rainstorm. Bulletin Of
643 Science and Technology., 29, 24-29,86, 2013.
644 DOI: [10.3969/j.issn.1001-7119.2013.05.006](https://doi.org/10.3969/j.issn.1001-7119.2013.05.006).

645 Xu, J, M.: Satellite Imagery Characteristics for Extratropical Cyclones and Meiyu Font.
646 Advances in Meteorological Science and Technology., 11, 14-26, 2021. DOI:
647 [10.3969/j.issn.2095-1973.2021.03.003](https://doi.org/10.3969/j.issn.2095-1973.2021.03.003)

648 Xu, Y, C., Wei, J, S. and Zhu, W, J.: A numerical simulation and marine sensitive
649 experiments of Jiang-Huai cyclone. J Meteor Sic., 31, 726-731, 2011.
650 DOI: [10.3969/j.issn.1009-0827.2011.06.008](https://doi.org/10.3969/j.issn.1009-0827.2011.06.008)

651 Yan, J, R., Wang, W, J., Zhang, H. and Shi, D, W.: Analysis of two rainstorm and gale
652 processes of Jianghuai cyclone in Jiangsu Province in 2019. Journal of

653 Meteorological Research and Application., 42, 83-88, 2021.
654 DOI: [10.19849/j.cnki.CN45-1356/P.2021.2.16](https://doi.org/10.19849/j.cnki.CN45-1356/P.2021.2.16)

655 Yang, Y, M., Gu, W, L., Zhao, R, L. and Liu, J.: The statical analysis of vortex during
656 Meiyu season in the lower reaches of the Yangtze. Quarterly Journal of Applied
657 Meteorology., 21, 11-18, 2010. DOI: [10.3969/j.issn.1001-7313.2010.01.002](https://doi.org/10.3969/j.issn.1001-7313.2010.01.002)

658 Zhao, B, K., Wu, G, X. and Yao, X, P.: A diagnostic analysis of potential vorticity
659 associated with development of a strong cyclone during the Meiyu period of 2003.
660 Chinese Journal of Atmospheric Sciences., 32, 1241-1255, 2008.
661 Doi: [10.3878/j.issn.1006-9895.2008.06.02](https://doi.org/10.3878/j.issn.1006-9895.2008.06.02).

662 Zhao, B, k., Wan, R, J. and Lu, X, Q.: A Contrastive Analysis on the Causes of Strong
663 and Weak Cyclones over Yangtze-Huaihe River Valleys during the Meiyu Period in
664 Summer of 2003. Plateau Meteorology., 29, 309-320, 2010.

665 Zhao, J, H., Chen, L, J. and Wang, D, Q.: Characteristics and causes analysis of
666 abnormal Meiyu in China in 2016. Chinese Journal of Atmospheric Sciences., 42,
667 1055-1066, 2018. DOI: [10.3878/j.issn.1006-9895.1708.17170](https://doi.org/10.3878/j.issn.1006-9895.1708.17170)

668 Zhao, J, H., Zhang, H., Zuo, J, Q., Xiong, K, G. and Chen, L, J.: What Drives the Super
669 Strong Precipitation over the Yangtze–Huaihe River Basin in the Meiyu Period of
670 2020. Chinese Journal of Atmospheric Sciences., 45, 1433–1450, 2021.
671 Doi: [10.3878/j.issn.1006-9895.2104.2101](https://doi.org/10.3878/j.issn.1006-9895.2104.2101).

672 Zhang, X, L., Tao, S, Y. and Zhang, S, L.: Three Types of Heavy Rainstorms Associated
673 with the Meiyu Front. Chinese Journal of Atmospheric Sciences, 28., 187-205, 2004.
674 doi: [10.3878/j.issn.1006-9895.2004.02.03](https://doi.org/10.3878/j.issn.1006-9895.2004.02.03)

675 Zhang, X, L., Tao, S, Y. and Zhang, Q, Y.: An Analysis on Development of MESO- β
676 Convective System along Meiyu Front Associated with Flood in Wuhan in 20-21
677 July 1998, Journal of Applied Meteorological Science., 13, 385-397, 2002. DOI:
678 [10.3969/j.issn.1001-7313.2002.04.001](https://doi.org/10.3969/j.issn.1001-7313.2002.04.001).

679 Zhang, X, H., Luo, J., Chen, X., Jin, L, L. and Qiu, X, M.: Formation and development
680 mechanism of one cyclone over Changjiang-Huaihe River basin and diagnostic
681 analysis of rainstorm. Meteor Mon., 42, 716-723, 2016.

682 DOI: [10.7519/j.issn.1000-0526.2016.06.007](https://doi.org/10.7519/j.issn.1000-0526.2016.06.007)

683 Zhang, J, G., Wang, J., Wu, T., Zhou, J, L., Zhong, M., Wang, S, S., Huang, X, Y., Li,
684 S, J., Han, F, R. and Wang, X, C.: Weather system types of extreme precipitation in
685 the middle reaches of the Yangtze River. *Torrential Rain and Disasters.*, 37, 14-23,
686 2018.

687 Doi: [10.3969/j.issn.1004-9045.2018.01.003](https://doi.org/10.3969/j.issn.1004-9045.2018.01.003)

688 Zhang, Y, X., Ding, Y, H. and Li, Q, P.: Cyclogenesis Frequency Changes of
689 Extratropical Cyclones in the Northern Hemisphere and East Asia Revealed by
690 ERA40 Reanalysis Data. *Meteor Mon.*, 38, 646-656, 2012.

691 Zhou, J, L., Zhang, J, G., Wu, T., Xu, G, Y., Liu, X, W., Wang, J. and Han, F, R.:
692 Characteristics of the mesoscale weather system producing extreme rainstorm in
693 boundary layer during the Meiyu front over the middle reaches of Yangtze River.
694 *Meteor Mon.*, 48, 1007-1019, 2022. DOI: [10.7519/j.issn.1000-0526.2022.052801](https://doi.org/10.7519/j.issn.1000-0526.2022.052801)

695 Zhong, Q, M., Ma, J., Wang, L.: Biweekly oscillation of the Meiyu-season precipitation
696 in 2016 and 2020 over the Yangtze Huaihe River basin: A comparative analysis. *Acta*
697 *Meteorologic Sinica.*, 8, 235-25, 2023. DOI: [10.11676/qxxb2023.20220075](https://doi.org/10.11676/qxxb2023.20220075)

698 Zhou, X, M., Zheng, Y, G.: Analysis of Environmental Conditions and Tornado Storm
699 Features of Two Tornadoes in Jiangsu during the Meiyu Period in 2020. *Advances in*
700 *Meteorological Science and Technology.*, 10, 34-42, 2020.

701 DOI: [10.3969/j.issn.2095-1973.2020.06.008](https://doi.org/10.3969/j.issn.2095-1973.2020.06.008).

702 Zhou, Y, , Xia, L.: Statistical Research on Climatic Characteristics of Jianghuai
703 Cyclones. *Meteorological and Environmental Sciences.*, 40, 79-85, 2017.

704 DOI: [10.16765/j.cnki.1673-7148.2017.03.013](https://doi.org/10.16765/j.cnki.1673-7148.2017.03.013)

705 Zhu, M., Lu, H, C. and Yu, Z, H.: Study of Positive Feedback Mechanism for Meso- α
706 Scale Cyclone Growing on Meiyu Front. *Chinese Journal of Atmospheric Sciences.*,
707 22, 763-770, 1998. Doi: [10.3878/j.issn.1006-9895.1998.05.11](https://doi.org/10.3878/j.issn.1006-9895.1998.05.11)